

THE ULTRAVIOLET PEAK OF THE ENERGY DISTRIBUTION IN 3C 273: EVIDENCE FOR AN ACCRETION DISK AND HOT CORONA AROUND A MASSIVE BLACK HOLE

GERARD A. KRISS^{1,2}, ARTHUR F. DAVIDSEN², WEI ZHENG², AND GEUNHO LEE^{2,3}

To appear in the 1999 December 20 issue of the Astrophysical Journal

ABSTRACT

We present absolutely calibrated far-ultraviolet spectrophotometry of the quasar 3C 273 covering the 900–1800 Å range. Our ~ 3 Å resolution spectra were obtained with the Hopkins Ultraviolet Telescope during the Astro-1 mission in December 1990 and during the Astro-2 mission in March 1995. Both spectra exhibit a change in slope near the Lyman limit in the quasar rest frame. At longer UV wavelengths, the continuum has a power-law index of 0.5–0.7, while shortward of the Lyman limit it is 1.2–1.7. The energy distribution in νf_ν therefore peaks close to the quasar Lyman limit. The short wavelength UV power law extrapolates well to match the soft X-ray excess seen in simultaneous observations with the Broad-Band X-ray Telescope and nearly simultaneous ROSAT observations.

The general shape of the broad-band spectrum of 3C 273 is consistent with that of an optically thick accretion disk whose emergent spectrum has been Comptonized by a hot medium. Our UV spectrum is well described by a Schwarzschild black hole of $7 \times 10^8 M_\odot$ accreting matter at a rate of $13 M_\odot \text{ yr}^{-1}$ through a disk inclined at 60 degrees. Superposed on the intrinsic disk spectrum is an empirically determined Lyman edge of optical depth 0.5. The Comptonizing medium has a Compton parameter $y \approx 1$, obtained with an optical depth to electron scattering of unity and a temperature of 4×10^8 K.

This overall shape is the same as that found by Zheng et al. and Laor et al. in their UV and X-ray composite spectra for quasars, giving physical validity to the composite spectrum approach. When combined with those results, we find that the generic ionizing continuum shape for quasars is a power law of energy index 1.7–2.2, extending from the Lyman limit to ~ 1 keV. The observational gap in the extreme ultraviolet for these combined data describing the quasar continuum shape is now only half a decade in frequency.

Subject headings: Accretion Disks — Galaxies: Quasars: General — Galaxies: Quasars: Individual (3C 273) — Ultraviolet: Galaxies

1. INTRODUCTION

It has long been known that the energy distribution of quasars, expressed as νL_ν , must have a peak somewhere in the far-ultraviolet to soft X-ray region of the spectrum. Shields (1978) first suggested that the optical and near UV flux of quasars might be due to the Rayleigh-Jeans portion of a black body spectrum whose peak lies in the unobserved extreme UV region, arising from an optically thick accretion disk surrounding a massive black hole (Lynden-Bell 1969), and dubbed the “big blue bump.” This idea was then further developed and applied to UV observations of quasars obtained with IUE (Malkan & Sargent 1982; Malkan 1983). It was subsequently found that the X-ray spectra of quasars also showed a “soft excess” of flux, above the extrapolation of the relatively flat power-law that fit the spectrum at energies above 2 keV (Turner & Pounds 1988; Masnou et al. 1992), and which might arise from the Wien portion of the same thermal spectrum. In addition to whatever light this spectral region might shed on the black-hole accretion-disk model for quasars, it is also a fundamental input to studies of the photoionization of the broad emission line clouds in quasars (Krolik & Kallman 1988) as well as the photoionization of the intergalactic medium (Haardt & Madau 1996). Consequently there has been widespread interest in determining the detailed shape of the spectrum of quasars between the optical (10^{15} Hz)

and the soft X-ray (10^{17} Hz), and in particular, establishing more precisely where in the extreme UV the peak of the big blue bump is located (Arnaud et al. 1985; Bechtold et al. 1987; O’Brien, Gondhalekar, & Wilson 1988).

The quasar 3C 273 provides an excellent candidate for addressing this problem because of its low redshift ($z=0.158$) and its high flux at both UV and X-ray wavelengths. It was the first quasar detected in X-rays (Bowyer et al. 1970) and also the first quasar observed in the far-ultraviolet (Davidson, Hartig, & Fastie 1977), both detections having been achieved with sounding rocket experiments before the advent of effective satellite observatories.

At X-ray energies the spectrum of 3C 273 in the 2–10 keV range is well fit by a power-law, $F_\nu \propto \nu^{-\alpha}$, with energy index $\alpha \approx 0.5$ (Worrall et al. 1979), but observations at lower energies with EXOSAT and *Ginga* (Turner et al. 1985, Courvoisier et al. 1987, Turner et al. 1990), *Einstein* (Wilkes & Elvis 1987, Turner et al. 1991, Masnou et al. 1992), and ROSAT (Staubert et al. 1992; Leach, McHardy, & Papadakis 1995, hereafter LMP95) have established the existence of a soft excess. Reporting on simultaneous observations of 3C 273 in 1990 December with ROSAT (0.1–2 keV) and *Ginga* (2–10 keV), Staubert et al. (1992) obtained a good fit with the sum of two power laws, with $\alpha = 0.56$ dominating at high energies and $\alpha = 2.5$ at low energies. However, the soft component could

¹Space Telescope Science Institute, 3700 San Martin Drive, Baltimore, MD 21218; gak@stsci.edu

²Center for Astrophysical Sciences, Department of Physics and Astronomy, The Johns Hopkins University, Baltimore, MD 21218–2686; afd@pha.jhu.edu, zheng@pha.jhu.edu

³Radio Research Laboratory, 370-9, Sinpilli, Seolseong-Myun, Ichon, Kyoungki-do, 467-880 Korea; lgh@solaradio.rrl.go.kr

TABLE 1
OBSERVATION LOG

	Instrument	Date Start Time (GMT)	Exposure (sec)	Comment
Astro-1	HUT	1990 December 05 23:28:24	1251	
		1990 December 09 17:23:54	2138	
	BBXRT	1990 December 09 17:37:01	1598	
	IUE SWP40331	1990 December 14	1800	
	SWP40333		1500	
	LWP19411		1800	
	LWP19412		1800	
	SWP40391	1990 December 19	1800	
	SWP40392		1800	
	LWP19447		1800	
	LWP19448		1620	
	ROSAT	1990 December 18–21	497	
	KPNO 2.1m	1990 December 05	60	
AA				
Astro-2	HUT	1995 March 12 06:05:03	1180	Flux correction 1.02
		1995 March 15 07:11:43	1304	Flux correction 1.05

also be modeled with a black body spectrum or with thermal bremsstrahlung (Staubert et al. 1992). More extensive observations of 3C 273 with ROSAT have been reported by LMP95. They established that “two physically distinct emission components are present”, with the spectrum best modeled by a combination of two power-laws with absorption by the Galactic column of gas, $N_H = 1.84 \times 10^{20} \text{ cm}^{-2}$. Constraining the harder component to have $\alpha_h = 0.5$ as observed by EXOSAT and *Ginga*, the soft component was found to be significantly steeper, with $\alpha_s = 1.7$ for most of the observations. Attempts to fit the soft component with various other models, including blackbody and bremsstrahlung radiation were found unacceptable (LMP95).

At ultraviolet wavelengths the first determination of the spectral index of 3C 273 (Davidsen, Hartig, & Fastie 1977) gave $\alpha = 0.6$ over the range from the optical to Lyman α , with a broad bump around 3500 Å, perhaps associated with Balmer continuum and Fe II line emission (Baldwin 1975), that has sometimes been called the “small blue bump”. It was also pointed out by Davidsen et al. that the spectral index must increase to $\alpha > 1.2$ somewhere near or above the Lyman limit in order to agree with the X-ray observations. Subsequent extensive observations with IUE give $\alpha = 0.66$ between 3100 and 1250 Å (Zheng & Malkan 1993). A very low resolution observation with the Voyager UV Spectrometer in the 900–1200 Å band suggested the possibility of a spectral break at about 1000 Å (Reichert et al. 1988), perhaps associated with the Lyman edge. Recent observations in the 900–1200 Å region with ORFEUS imply a turnover in the spectrum of 3C 273 near the IUE/ORFEUS transition wavelength at about 1200 Å (Appenzeller et al. 1998).

Here we report the results of observations of 3C 273 in the 900–1800 Å region made with the Hopkins Ultraviolet Telescope (HUT) on both the Astro-1 and Astro-2 space shuttle missions. The Astro-1 far-ultraviolet data are accompanied by con-

temporaneous observations at optical, ultraviolet, and soft and hard X-rays, yielding a quasi-simultaneous broad-band spectrum for this quasar extending over more than 3 decades of frequency. The HUT data alone show a definite spectral break, with a peak in the energy spectrum νL_ν at about 920 Å in the rest frame. The best-fit power-law at shorter wavelengths from 920 Å to 787 Å, when extrapolated, nearly matches the simultaneous soft X-ray spectrum. The Astro-2 HUT data are of even higher quality than those obtained on Astro-1 and yield similar results, confirming that the peak of the “big blue bump” has now definitely been seen in 3C 273. A comparison of these data with a composite quasar spectrum in the ultraviolet (Zheng et al. 1997) and the X-ray bands (Laor et al. 1997), suggests strongly that a peak in the energy spectrum of all quasars occurs near the Lyman limit, and that the ionizing continuum from the Lyman limit to 1 keV is a power-law of $\alpha = 1.7 - 2.2$.

2. OBSERVATIONS

The Hopkins Ultraviolet Telescope (HUT) incorporates a 0.9-m primary mirror and a prime-focus Rowland circle spectrograph as described by Davidsen et al. (1992) and Kruk et al. (1995). First-order spectra recorded by the photon counting detector cover the 820–1840 Å spectral range with a sampling of about 0.52 Å per pixel and a point source resolution of about 3 Å. Absorption by interstellar hydrogen limits the observed spectra to wavelengths longer than the Lyman limit at 912 Å (787 Å in the quasar rest frame).

HUT was used to observe 3C 273 on the Astro-1 space shuttle mission in 1990 December and again on the Astro-2 mission in 1995 March. The performance and calibration of the instrument are described for Astro-1 by Davidsen et al. (1992) and Kruk et al. (1997) and for Astro-2 by Kruk et al. (1995, 1999). Because substantial changes to HUT’s performance were made between the two flights, the results of the spectrophotometric observations may be regarded as independent measurements,

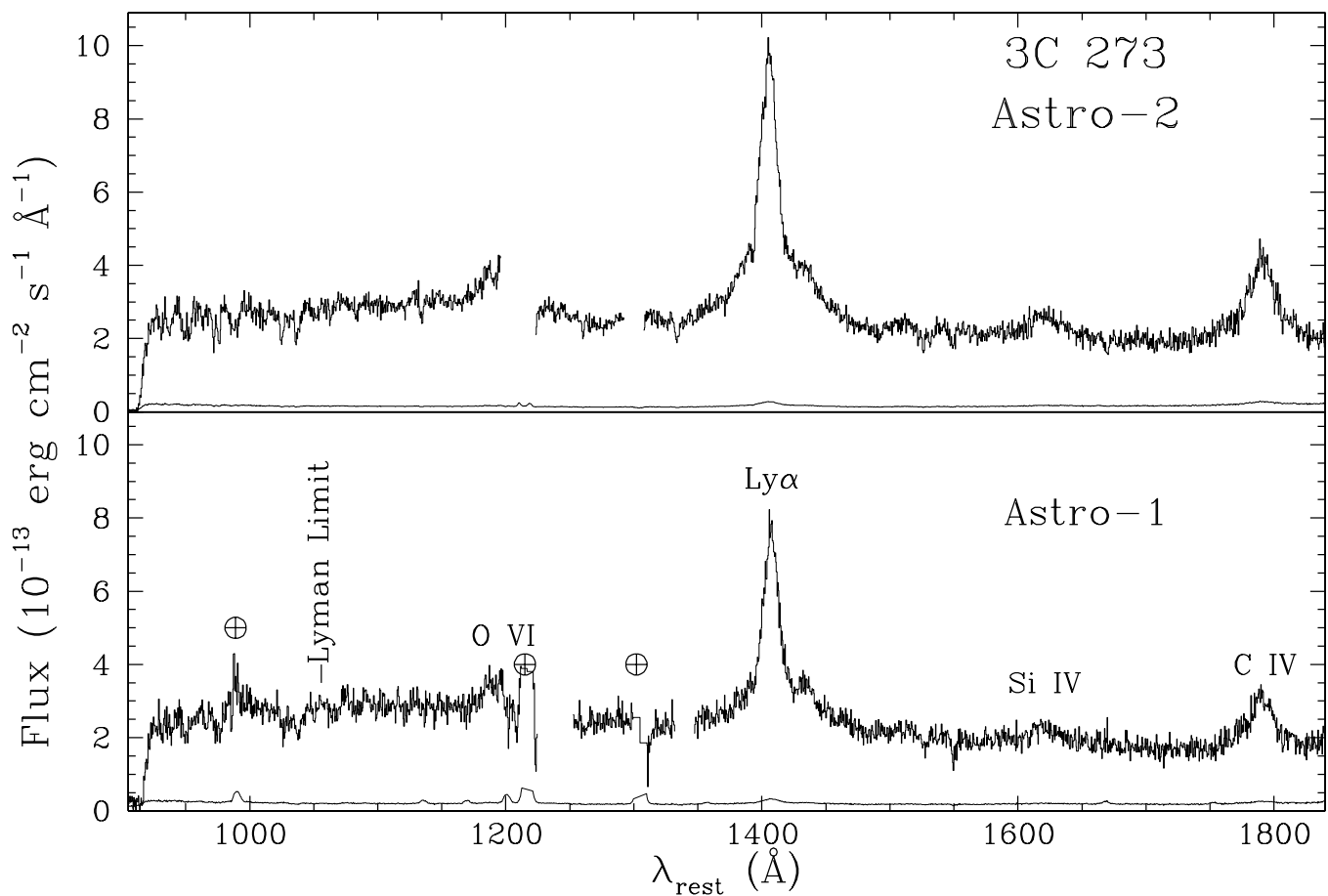


FIG. 1.— 3C 273 spectrum (histogram) from 900 to 1820 Å as observed with HUT on Astro-1 (lower panel) and Astro-2 (upper panel). Pixels are about 0.51 Å and the resolution is about 3 Å. Curves at the bottom of each panel give the values of the error array produced by the standard HUT reduction process. Strong peaks in the 1σ error array for Astro-1 correspond to strong geocoronal emission lines (airglow) for this observation, obtained mostly in daylight. Airglow lines have been subtracted using templates developed from blank sky observations, and their positions are marked with \oplus . The Astro-2 spectrum was obtained at night, resulting in much weaker airglow. Emission and absorption lines are marked.

effectively produced by two different instruments. The Astro-1 observations were (necessarily) conducted primarily during daylight portions of the shuttle orbit, where there is substantial contamination by geocoronal emission lines that must be subtracted in the data reduction process. The Astro-2 observations, however, were obtained mostly during night-time portions of the orbit, where the geocoronal contamination is greatly reduced. Only the night portion of the Astro-2 data is used. Details of the observations are given as an observation log in Table 1.

For Astro-1 there are several nearly simultaneous observations that can be used to determine the broad-band spectrum of 3C 273. Also mounted on the shuttle with HUT was the Broad Band X-Ray Telescope (BBXRT) (Serlemitsos et al. 1992), which observed 3C 273 in the 0.3–12 keV band with a resolution of about 100 eV. ROSAT observations in the 0.1–2.4 keV band were obtained less than two weeks after the Astro-1 observations (Staubert et al. 1992), and *Ginga* observations in the 2–20 keV band were also obtained during 1990 December (Staubert et al. 1992). In the ultraviolet, IUE spectra in both the short and long wavelength cameras were obtained between one and two weeks after the HUT observations, and these have been extracted from the IUE archive. Finally, an optical spectrum of 3C 273 was kindly obtained for us by R. Green on the KPNO 2.1 m telescope during the Astro-1 mission. All these

contemporaneous measurements are listed in the observation log in Table 1.

The HUT observations of 3C 273 from Astro-2 in 1995 March are also listed in Table 1. Unfortunately, we have been unable to find any nearly simultaneous observations at other wavelengths for this epoch.

3. RESULTS FROM THE HUT OBSERVATIONS

3.1. Observed Spectra

The two HUT observations of 3C 273 from Astro-1 were summed and then processed and reduced to an absolute flux scale following our standard procedures as described by Kruk et al. (1997). For Astro-2 the two observations were reduced separately because of the variation of the instrument sensitivity during the mission (Kruk et al. 1995), and the resulting spectra were then averaged, weighted by their exposure time, to yield the final spectrum presented here. As noted in Table 1, the Astro-2 data had slight flux corrections of 2–5% applied due to light loss at the slit induced by pointing errors. The results for both missions are displayed in Fig. 1.

It is worth emphasizing that the Astro-1 and Astro-2 spectra were obtained, reduced, and calibrated under markedly different circumstances. The Astro-1 data were obtained with an instrument of relatively modest sensitivity, almost entirely during

orbital day when there is substantial contamination by geocoronal emission lines that must be subtracted, and were absolutely calibrated by reference to an observation of the DA white dwarf G191-B2B using a model atmosphere computed for this star by P. Bergeron (Davidsen et al. 1992). The Astro-2 data, on the other hand, were obtained with an instrument of much higher sensitivity, entirely during orbital night with minimal geocoronal contamination, and were absolutely calibrated by reference primarily to observations of the DA white dwarf HZ43 using a model atmosphere computed by D. Finley using D. Koester's model atmosphere codes (Kruk et al. 1995). In spite of these major differences, the resulting spectra in Fig. 1 are remarkably similar. Of course, 3C 273 is known to vary, so the close agreement between observations made more than four years apart is fortuitous. Indeed there are clear changes observed both in the continuum and in the emission line strengths (discussed below). However, both spectra show a change of continuum slope near the Lyman limit in the rest frame of the quasar, which is further discussed in the next section.

3.2. Empirical Models for the Spectra

We first remove the airglow lines from the spectra. We use a geocoronal Ly α template that is derived from blank fields and scaled by the exposure time, and subtract it from the HUT spectrum of 3C 273. Other airglow lines are fitted and removed, but significant residuals still exist in the regions around the strongest airglow lines at 1216, 1302 and 989 Å.

We use the IRAF task *specfit* (Kriss 1994) to fit both the Astro-1 and Astro-2 spectra with various components for the continuum, emission lines and absorption features. We use the same overall model for both spectra, and identical fitting windows spanning the wavelength intervals 912–1194, 1238–1287, and 1319–1820 Å. For the Astro-1 data, we also model the remaining airglow residuals near 989 Å.

The intrinsic emission lines of Ly α , C IV and O VI are modeled with dual Gaussians, and other emission components are modeled with single Gaussians. We constrain many components of the fit by tying related parameters together. The full-widths at half maximum (FWHM) of the weaker broad emission lines (S VI, C III, N III, O I, C II) are all linked, and their wavelengths are linked to that of narrow Ly α by the ratio of their laboratory wavelengths. The FWHM of broad O VI λ 1034 is linked to broad C IV λ 1549. The wavelengths and FWHM of the N V components are linked to the corresponding C IV components. We include one unidentified weak, broad emission feature at a rest wavelength of 1074 Å. This is not He II λ 1085, and it is approximately at the location of the unidentified feature also seen in Faint Object Spectrograph (FOS) observations by Laor et al. (1995).

For the absorption lines, we start by including features identified in previous, higher resolution observations (FOS: Bahcall et al. 1991; GHRS: Morris et al. 1991; ORFEUS: Hurwitz et al. 1998). We then add additional features as required to obtain a good fit to the HUT data. As with the emission lines, we constrain many components of the fit by tying the FWHM of the lines together in groups by wavelength regions where the instrumental resolution is roughly the same. All lines are assumed to be unresolved, except for the blend of O VI, C II, and O I around 1038 Å, the blended Si II lines at 1192 Å, and the blended C IV doublet at 1549 Å.

The wavelength region below 950 Å is heavily absorbed by the high-order lines of Galactic hydrogen. To model this,

we use a set of absorption profiles, each including 50 Lyman-series lines, with a fixed column density of $1.8 \times 10^{20} \text{ cm}^{-2}$. The absorption lines are modeled using Voigt profiles covering a range of 10–20 km s $^{-1}$ in the Doppler parameter which are then convolved with the instrument resolution, a Gaussian of 3 Å FWHM. For our extinction correction, we adopt $E(B-V) = 0.032$, as established by Lockman & Savage (1995), and use the extinction curve of Cardelli, Clayton & Mathis (1989), with $R_V = 3.1$. This value of the extinction is also consistent with the $E(B-V) = 0.03$ adopted by Lichti et al. (1995) and Appenzeller et al. (1998).

For both the Astro-1 and Astro-2 spectra, we obtain our best fit using a broken power-law model for the continuum shape. To ascertain the significance of the apparent spectral break near the Lyman limit, we compare fits performed using a single power-law for the continuum shape to a broken power-law. The single power-law fits are summarized in Table 2, and the broken power-law fits are summarized in Table 3. For the Astro-1 data, the fits with a single power law do not produce satisfactory results. These fits are shown as smooth curves in Fig. 2 and Fig. 3. Note that the single power-law fit deviates significantly at wavelengths shortward of 1200 Å. Even allowing for reddening corrections higher than the Galactic value, the fits are still poor, as shown in Table 2. The spectral break in the sub-Ly α region is too sharp to be accounted for by reddening.

TABLE 2
SINGLE POWER-LAW FITS TO 3C 273

$E(B-V)$	Astro-1		Astro-2	
	α	χ^2/dof	α	χ^2/dof
0.01	0.94	1689/1544	1.16	1723/1501
0.02	0.81	1651/1544	1.00	1698/1501
0.032	0.62	1619/1544	0.79	1697/1501
0.04	0.49	1615/1544	0.67	1708/1501
0.05	0.34	1602/1544	0.50	1746/1501
0.06	0.18	1607/1544
0.08	-0.15	1650/1544

TABLE 3
BROKEN POWER-LAW FITS TO 3C 273^a

Parameter	Astro-1	Astro-2
f_0^b	4.37 ± 0.04	4.41 ± 0.02
λ_0 (Å)	1064 ± 8	1036 ± 6
α_1	1.69 ± 0.16	1.19 ± 0.15
α_2	0.46 ± 0.03	0.74 ± 0.02
χ^2/dof	1584/1542	1692/1499

^a Assumes extinction fixed at $E(B-V) = 0.032$.

^b Measured at the break wavelength λ_0 , in units of $10^{-13} \text{ ergs s}^{-1} \text{ cm}^{-2}$.

Although the Astro-2 spectrum is fairly similar to the Astro-1 data, the continuum shape is noticeably less blue at wavelengths longward of Ly α , and the broad emission lines are significantly brighter. One can see this most easily in the comparison of the fitted spectra shown in Fig. 4. Since the Astro-2 spectrum is not as blue, the break at shorter wavelengths is not as dramatic, and a single power law reddened at the nominal Galactic value fits only slightly worse than the broken power law as one can see in the top panels of Figures 2 and 3. Thus, we conclude that a short wavelength spectral break is required by our Astro-1 data, but not by the Astro-2 data.

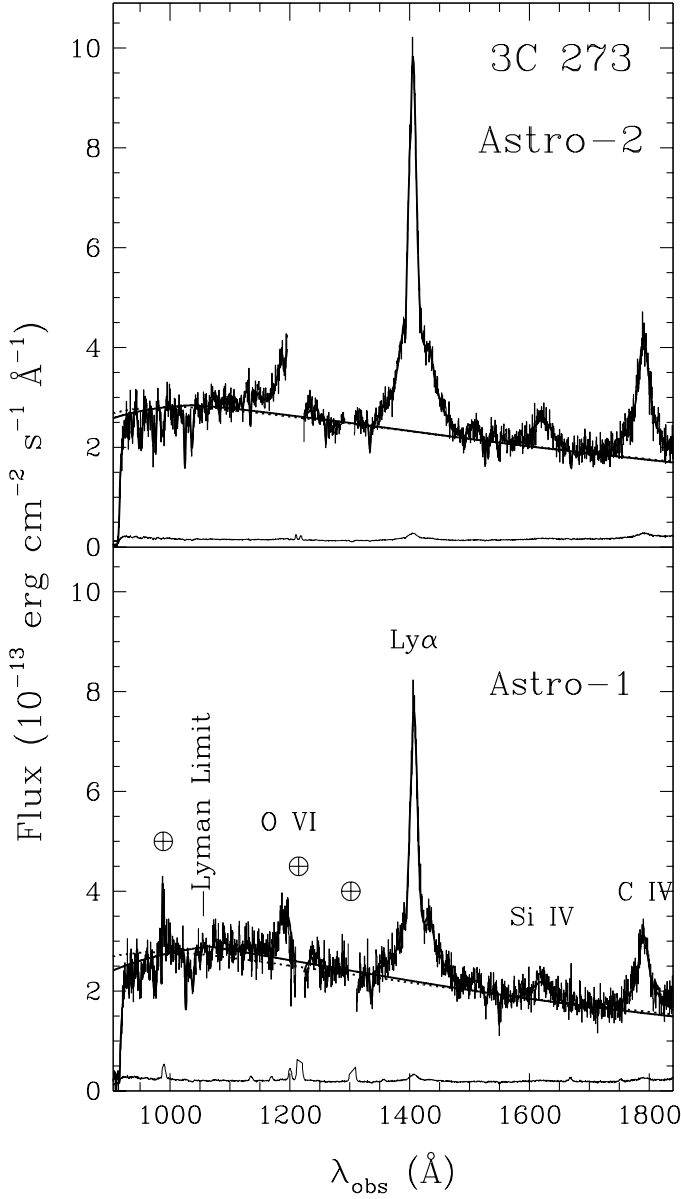


FIG. 2.— Observed spectra of 3C 273 with the best-fitting empirical models as described in Section 3.2. The models include emission and absorption lines and a continuum described either by a single power-law (dotted line) or by a broken power-law (solid lines). Reddening with $E(B-V) = 0.032$ is applied to the models. Broken power-laws provide the best fit for both spectra. A single power-law gives an unacceptable fit for the Astro-1 spectrum; for Astro-2 a single power-law is worse, but acceptable. Parameters of the models are given in Tables 2–7.

As the broken power law continuum models give our best fits for both data sets, we quote the parameters for the emission and absorption lines using these continuum models. Tables 4 and 5 give the observed wavelengths, the observed fluxes, and full-widths at half-maximum (FWHM) for the Astro-1 and Astro-2 observations of the emission lines, respectively. Tables 6 and 7 list the observed wavelengths, equivalent widths (W_λ), and FWHM for the absorption lines. None of the line widths are corrected for the instrumental resolution. For all absorption lines, the best-fit widths are consistent with the instrumental resolution and should therefore be considered unresolved. The error bars quoted on all parameters are determined from the

error matrix of the fit, and they represent the 1σ confidence interval for a single interesting parameter (Kriss 1994).

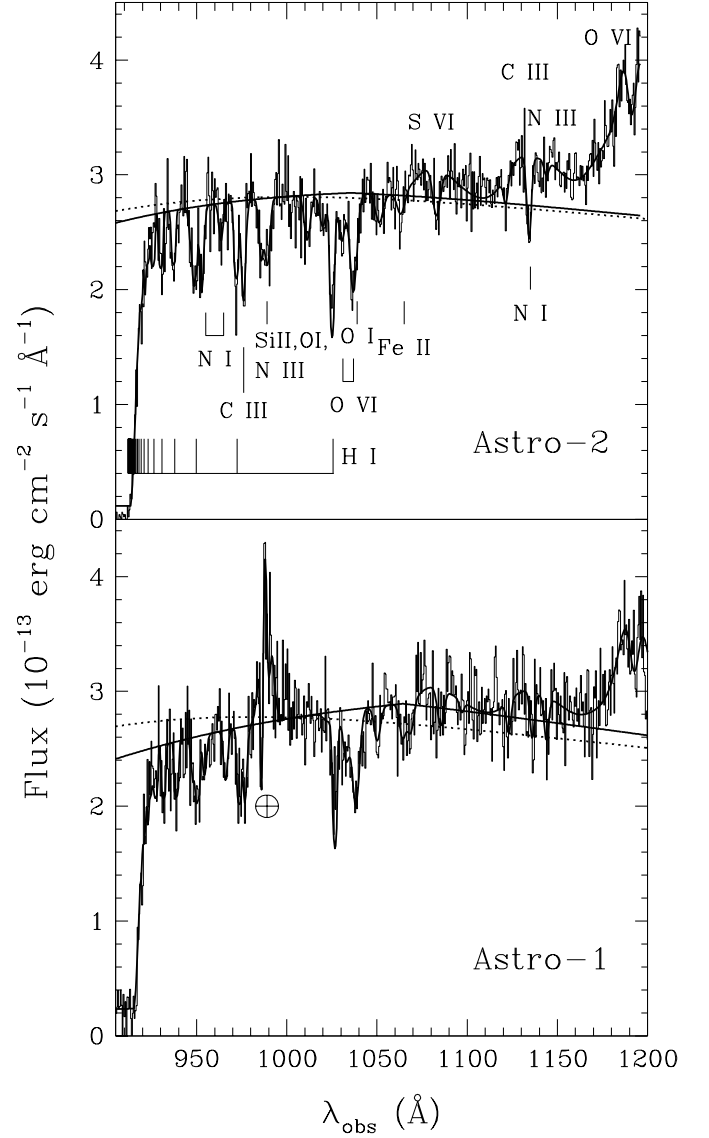


FIG. 3.— Same as Fig. 2 but showing the crucial 900–1200 Å region at an enlarged scale. Positions of the Lyman series of interstellar hydrogen absorption lines are indicated. Series lines up to L7 are clearly seen in the data. The continuum in this region is well-fit by the broken power-law model (solid curves), while the best single power-law model (dotted) lies above the data at the shortest wavelengths.

4. THE BROAD-BAND SPECTRUM OF 3C 273

The BBXRT data were obtained simultaneously with the Astro-1 HUT data, and we have retrieved them from the National Space Science Data Center (NSSDC) archive. To obtain the unfolded X-ray spectrum, we use the data reduction package *xspec* (Arnaud 1996). The data points in channels 1–20 and 450–512 are excluded because of high uncertainties. We bin the data so that each bin has at least 20 counts. Our preliminary fits with single power laws or broken power laws yielded poor fits, with a significant deviation around 0.6 keV. Done (1993) suggests that this is a blueshifted O VIII resonance absorption feature. Empirically modeling this feature as an absorption edge, we use a dual power-law with fixed Galactic absorption

to model the X-ray spectrum:

$$dN/dE = (f_1 E^{-\alpha_1} + f_2 E^{-\alpha_2}) \exp(-\tau(E/E_{th})^{-3}) \exp(-\tau(N_H, E)).$$

This model gives a good fit ($\chi^2 = 52.5$ for 52 binned data points and 6 free parameters). The parameters for our best fit are: the photon power-law index $\alpha_1 = 4.3 \pm 0.9$, $\alpha_2 = 1.64 \pm 0.09$; flux at 1 keV: $f_1 = 0.0081 \pm 0.0030$ and $f_2 = 0.017 \pm 0.0025$ photon $s^{-1} cm^{-2} keV^{-1}$; and the absorption edge at $E_{th} = 0.51 \pm 0.03$ keV with an optical depth $\tau = 1.17 \pm 0.31$. This fit and the residuals are shown in Fig. 5.

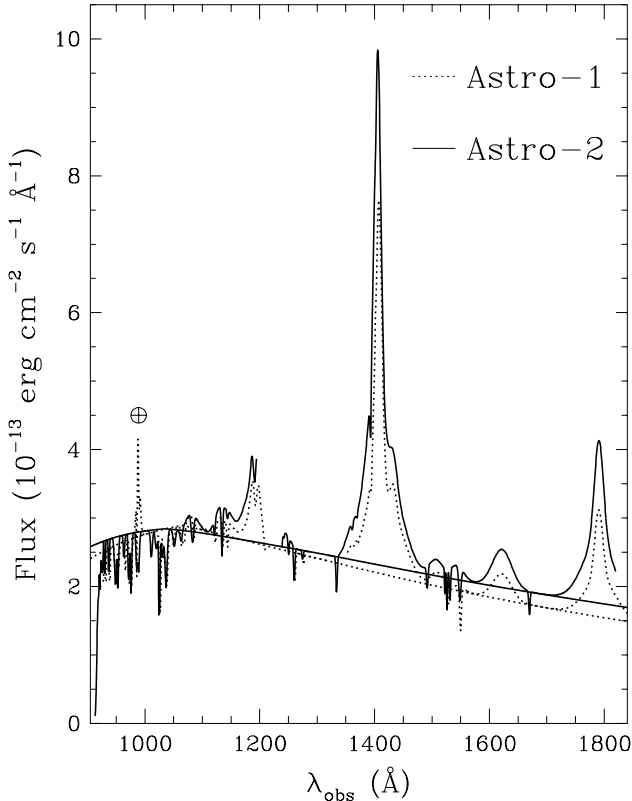


FIG. 4.— Direct comparison of the fits to the HUT Astro-1 (dotted lines) and Astro-2 (solid lines) spectra. Although the continuum fluxes are roughly the same, there are clear differences in the line fluxes and continuum shapes.

The nearly simultaneous optical, ultraviolet, and X-ray data collected in 1990 December during or shortly after the Astro-1 mission were listed in Table 1 and are shown in Fig. 6. The BBXRT and ROSAT data shown in Fig. 6 are corrected for Galactic absorption, using a Morrison & McCammon (1983) model with $N_H = 1.8 \times 10^{20} cm^{-2}$. (Note that we show *unfolded* X-ray data in Fig. 6, and that the plotted fluxes are model dependent.) Also shown is the power-law that best fits the short wavelength portion of the HUT spectrum as part of the broken power-law fit described in Section 3.2. This component has $\alpha = 1.7$. Two additional power-laws are also shown as dashed lines with indices of 1.7 ± 0.36 , representing the $1-\sigma$ errors from our fit added linearly to the uncertainty of ± 0.2 corresponding to a range in $E(B-V)$ of ± 0.01 , which is our estimate of the uncertainty in the extinction for 3C 273. It is clear from Fig. 6 and Fig. 2 that the energy distribution of 3C 273 peaks within the HUT spectral range, a little longward of the Lyman limit in the quasar rest frame, and that the short wavelength power-law that fits the HUT data extrapolates well to fit the soft X-ray data from ROSAT and BBXRT.

There still remains a considerable gap of one decade in frequency that cannot be filled for 3C 273, however, because the ultraviolet spectrum cannot be extended past the Galactic Lyman limit at 787 \AA in the quasar rest frame, and the soft X-ray spectrum is severely attenuated by interstellar absorption below 0.2 keV. Indeed this extreme ultraviolet gap cannot readily be decreased in the spectrum of any single quasar, since the higher redshifts that would allow the ultraviolet spectrum to be extended will at the same time limit the observed X-ray spectrum to higher rest-energies. We therefore turn to a composite quasar spectrum assembled from many different objects to try to reduce the size of the extreme ultraviolet gap.

In a previous paper (Zheng et al. 1997) we have presented the results of an analysis of HST FOS spectra of 101 quasars, most with redshifts from 0.33 to 1.5 , with a few high redshift objects with z up to 3.6 . The composite quasar spectrum was also fit with a broken power-law, the break occurring around 1050 \AA in the rest frame. The short wavelength component was found to have $\alpha = 2.0$ for the total sample (which is subject to unknown selection effects), while the subset of 60 radio-loud quasars had $\alpha = 2.2$ and the subset of 41 radio-quiet quasars had $\alpha = 1.8$.

In the lower panel of Fig. 6 we plot the radio-loud composite quasar spectrum from Zheng et al. (1997) scaled to match the flux observed for 3C 273 at 1000 \AA , near the break point in both spectra. Also shown as a solid line (with a break at 2 keV) is a composite quasar X-ray spectrum for radio-loud quasars from Laor et al. (1997), which has been scaled in flux to match our UV-optical composite using the average α_{ox} of 1.445 from the sample of Laor et al.

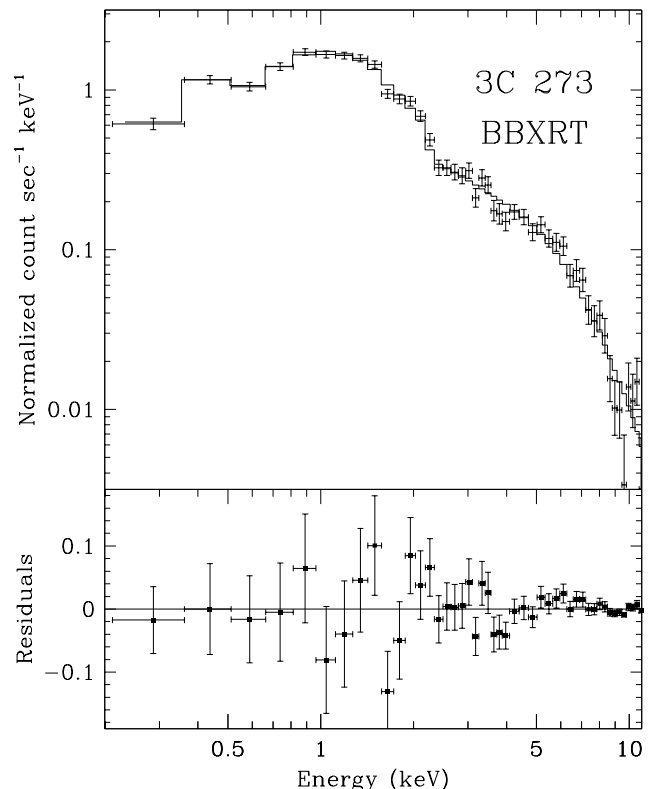


FIG. 5.— *Upper panel*: the best-fit model to the Astro-1 BBXRT X-ray spectrum. As described in §4, the solid line is a dual power law model with Galactic absorption and an empirical absorption edge at 0.5 keV folded through the BBXRT response function. The error bars are 1σ . *Lower panel*: residuals to the fit.

TABLE 4
ASTRO-1 EMISSION LINES

Feature	λ_{obs} (Å)	Flux ^a	FWHM (km s ⁻¹)
S VI, λ 933.38	1079.42 \pm 0.20	2.0 \pm 1.0	4905 \pm 721
S VI, λ 944.52	1092.32 \pm 0.20	1.0 \pm 0.5	4905 \pm 721
C III, λ 977.03	1129.95 \pm 0.20	3.8 \pm 1.2	4905 \pm 721
N III, λ 991.00	1146.12 \pm 0.20	2.9 \pm 1.1	4905 \pm 721
O VI, λ 1034.00	1191.46 \pm 0.20	16.1 \pm 3.9	4225 \pm 776
O VI, λ 1034.00	1191.46 \pm 0.20	13.7 \pm 5.5	10554 \pm 723
O VI, λ 1034.00 ^b	...	29.8 \pm 6.8	...
No ID	1243.66 \pm 1.15	5.3 \pm 1.1	4905 \pm 721
C III, λ 1175.70	1360.28 \pm 0.20	6.6 \pm 1.8	4905 \pm 721
Ly α , λ 1215.67	1406.21 \pm 0.20	56.3 \pm 3.8	2782 \pm 113
Ly α , λ 1215.67	1398.72 \pm 1.66	49.8 \pm 5.1	8375 \pm 733
Ly α , λ 1215.67 ^b	...	106.1 \pm 6.3	...
N V, λ 1240.15	1431.80 \pm 0.52	6.1 \pm 1.8	2782 \pm 308
N V, λ 1240.15	1434.68 \pm 1.89	41.0 \pm 3.8	10554 \pm 723
N V, λ 1240.15 ^b	...	47.1 \pm 4.2	...
O I, λ 1304.35	1508.05 \pm 0.20	5.8 \pm 1.1	4905 \pm 721
C II, λ 1335.30	1544.34 \pm 0.20	2.1 \pm 1.2	4905 \pm 721
Si IV, λ 1402.77	1620.89 \pm 1.62	15.1 \pm 2.4	6978 \pm 1325
C IV, λ 1549	1789.44 \pm 0.52	17.8 \pm 2.5	2782 \pm 308
C IV, λ 1549	1793.03 \pm 1.89	36.1 \pm 4.1	10554 \pm 723
C IV, λ 1549 ^b	...	53.9 \pm 4.8	...

^a10⁻¹³ erg cm⁻² s⁻¹

^bTotal flux for the narrow and broad components.

TABLE 6
ASTRO-1 ABSORPTION LINES

Feature	λ_{obs} (Å)	W_λ (Å)	FWHM ^a (km s ⁻¹)
O I, λ 948.69	947.09 \pm 0.41	0.4 \pm 0.2	820 \pm 162
N I blend, λ 953.00	953.28 \pm 0.41	0.4 \pm 0.2	820 \pm 162
P II, N I, λ 964.00	964.94 \pm 0.41	0.5 \pm 0.1	820 \pm 162
C III, λ 977.03	975.68 \pm 0.30	0.7 \pm 0.1	820 \pm 162
S III, λ 1012.50	...	< 0.2 ^b	1147
Si II, λ 1020.70	1020.70 \pm 0.30	0.1 \pm 0.1	1162 \pm 128
O VI, λ 1031.93	1031.93 \pm 0.29	0.6 \pm 0.1	1162 \pm 128
O VI, C II, O I, λ 1038.00	1037.19 \pm 0.29	1.5 \pm 0.1	1344 \pm 148
Ar I, λ 1048.22	1049.04 \pm 0.39	0.5 \pm 0.1	1162 \pm 128
Fe II, λ 1063.18	1063.18 \pm 0.39	0.5 \pm 0.1	1162 \pm 128
Ar I, λ 1066.66	1067.51 \pm 0.39	0.5 \pm 0.1	1162 \pm 128
N II, λ 1084.19	1084.19 \pm 0.72	0.5 \pm 0.2	1162 \pm 128
Fe II, λ 1096.88	...	< 0.2 ^b	779
Fe II, λ 1121.97	1121.97 \pm 0.72	0.3 \pm 0.1	779 \pm 127
N I, λ 1134.63	1134.96 \pm 0.72	0.4 \pm 0.2	779 \pm 127
Fe II, λ 1143.22	1142.81 \pm 0.72	0.4 \pm 0.1	779 \pm 127
Si II blend, λ 1192.00	1191.56 \pm 0.72	1.1 \pm 0.3	1536 \pm 497
N V, λ 1238.82	...	0.2 ^c	536
N V, λ 1242.80	...	0.1 ^c	536
S II, λ 1250.50	1250.40 \pm 0.29	0.5 \pm 0.1	536 \pm 137
S II, Si II, λ 1260.00	1260.43 \pm 0.67	0.4 \pm 0.1	536 \pm 137
H I, λ 1275.19	...	0.1 ^c	536
C II, λ 1335.30	1335.19 \pm 0.34	1.0 \pm 0.2	964 \pm 176
H I, λ 1361.42	...	0.1 ^c	964
Ni II, λ 1370.09	...	0.1 ^c	589
Si IV, λ 1393.76	1393.35 \pm 0.51	0.2 \pm 0.1	589 \pm 100
Si IV, λ 1402.77	1402.31 \pm 0.51	0.1 \pm 0.1	589 \pm 100
Si II, λ 1527.17	1526.25 \pm 0.56	0.7 \pm 0.2	826 \pm 225
C IV, λ 1549.50	1548.73 \pm 0.26	1.3 \pm 0.2	715 \pm 137
Al II, λ 1670.79	...	< 0.4 ^b	554

^aAll tabulated widths are consistent with the instrumental resolution, and all features should be considered unresolved.

^bThe upper limit for this line assumed a feature at the nominal wavelength with a fixed FWHM as shown.

^cOur fits included a feature at the nominal wavelength with the EW and FWHM fixed at the values shown.

TABLE 5
ASTRO-2 EMISSION LINES

Feature	λ_{obs} (Å)	Flux ^a	FWHM (km s ⁻¹)
S VI, λ 933.38	1079.59 \pm 0.15	4.2 \pm 0.2	5145 \pm 151
S VI, λ 944.52	1092.47 \pm 0.15	2.1 \pm 0.1	5145 \pm 151
C III, λ 977.03	1130.05 \pm 0.15	7.4 \pm 0.5	5145 \pm 151
N III, λ 991.00	1146.20 \pm 0.15	6.5 \pm 0.8	5145 \pm 151
O VI, λ 1034.00	1191.12 \pm 1.18	13.6 \pm 9.2	2332 \pm 590
O VI, λ 1034.00	1191.12 \pm 1.18	38.7 \pm 3.0	10416 \pm 477
O VI, λ 1034.00 ^b	...	52.3 \pm 9.6	...
No ID	1243.66 \pm 1.15	5.6 \pm 0.8	5145 \pm 151
C III, λ 1175.70	1360.08 \pm 0.15	10.0 \pm 1.0	5145 \pm 151
Ly α , λ 1215.67	1405.94 \pm 0.15	70.7 \pm 3.3	2799 \pm 76
Ly α , λ 1215.67	1399.49 \pm 0.70	93.5 \pm 4.4	8445 \pm 322
Ly α , λ 1215.67 ^b	...	164.2 \pm 5.5	...
N V, λ 1240.15	1433.61 \pm 0.40	6.6 \pm 1.6	3070 \pm 213
N V, λ 1240.15	1433.79 \pm 1.22	52.8 \pm 3.5	10416 \pm 477
N V, λ 1240.15 ^b	...	59.4 \pm 3.8	...
O I, λ 1304.35	1507.65 \pm 0.15	6.5 \pm 0.9	5145 \pm 151
C II, λ 1335.30	1543.90 \pm 0.15	5.3 \pm 1.3	5145 \pm 151
Si IV, λ 1402.77	1622.38 \pm 0.95	21.5 \pm 2.0	6800 \pm 671
C IV, λ 1549	1791.30 \pm 0.40	28.6 \pm 2.8	3070 \pm 213
C IV, λ 1549	1791.53 \pm 1.22	57.8 \pm 3.2	10416 \pm 477
C IV, λ 1549 ^b	...	86.4 \pm 4.2	...

^a10⁻¹³ erg cm⁻² s⁻¹

^bTotal flux for the narrow and broad components.

TABLE 7
ASTRO-2 ABSORPTION LINES

Feature	λ_{obs} (Å)	W_λ (Å)	FWHM ^a (km s ⁻¹)
O I, λ 948.69	947.61 \pm 0.47	0.4 \pm 0.1	894 \pm 130
N I blend, λ 953.00	953.28 \pm 0.22	0.8 \pm 0.1	894 \pm 130
P II, N I, λ 964.00	964.04 \pm 0.44	0.3 \pm 0.1	894 \pm 130
C III, λ 977.03	976.48 \pm 0.15	1.0 \pm 0.1	894 \pm 130
Si II, λ 989.87	989.31 \pm 0.15	0.5 \pm 0.1	894 \pm 130
N III, λ 991.00	990.44 \pm 0.15	0.3 \pm 0.1	894 \pm 130
S III, λ 1012.50	1011.80 \pm 0.47	0.6 \pm 0.1	1202 \pm 129
Si II, λ 1020.70	1020.29 \pm 0.62	0.4 \pm 0.1	1202 \pm 129
O VI, λ 1031.93	1031.00 \pm 0.41	0.6 \pm 0.1	1202 \pm 129
O VI, C II, O I, λ 1038.00	1037.43 \pm 0.21	1.6 \pm 0.1	1386 \pm 149
Ar I, λ 1048.22	1051.70 \pm 0.69	0.5 \pm 0.1	1410 \pm 318
Fe II, λ 1063.18	1063.74 \pm 0.67	0.4 \pm 0.1	1410 \pm 318
Ar I, λ 1066.66	...	< 0.2 ^b	1410
N II, λ 1084.19	1083.46 \pm 0.52	0.7 \pm 0.2	1410 \pm 318
Fe II, λ 1096.88	...	< 0.2 ^b	767
Fe II, λ 1121.97	1121.89 \pm 0.46	0.2 \pm 0.1	767 \pm 126
N I, λ 1134.63	1134.83 \pm 0.18	0.7 \pm 0.1	767 \pm 126
Fe II, λ 1143.22	...	< 0.2 ^b	767
Si II blend, λ 1192.00	1191.33 \pm 0.76	1.9 \pm 1.8	1654 \pm 513
N V, λ 1238.82	1238.91 \pm 0.77	0.2 \pm 0.1	588 \pm 143
N V, λ 1242.80	1242.60 \pm 0.77	0.1 \pm 0.1	588 \pm 143
S II, λ 1250.50	1250.63 \pm 0.64	0.2 \pm 0.1	588 \pm 143
S II, Si II, λ 1260.00	1260.75 \pm 0.20	0.5 \pm 0.1	588 \pm 143
H I, λ 1275.19	...	0.1 ^c	588
C II, λ 1335.30	1334.34 \pm 0.21	0.7 \pm 0.1	651 \pm 103
H I, λ 1361.42	...	0.1 ^c	651
Ni II, λ 1370.09	...	0.1 ^c	599
Si IV, λ 1393.76	1393.68 \pm 0.17	0.5 \pm 0.1	599 \pm 100
Si IV, λ 1402.77	1402.63 \pm 0.17	0.2 \pm 0.1	599 \pm 100
No ID, λ 1492.00	1492.28 \pm 0.54	0.4 \pm 0.1	599 \pm 100
No ID, λ 1522.00	1522.85 \pm 0.25	0.2 \pm 0.1	246 \pm 92
Si II, λ 1527.17	1526.68 \pm 0.17	0.7 \pm 0.1	453 \pm 96
No ID, λ 1533.00	1531.85 \pm 0.25	0.5 \pm 0.1	453 \pm 96
C IV, λ 1549.50	1549.23 \pm 0.33	1.0 \pm 0.2	884 \pm 147
Al II, λ 1670.79	1670.24 \pm 0.42	0.6 \pm 0.2	539 \pm 170

^aAll tabulated widths are consistent with the instrumental resolution, and all features should be considered unresolved.

^bThe upper limit for this line assumed a feature at the nominal wavelength with a fixed FWHM as shown.

^cOur fits included a feature at the nominal wavelength with the EW and FWHM fixed at the values shown.

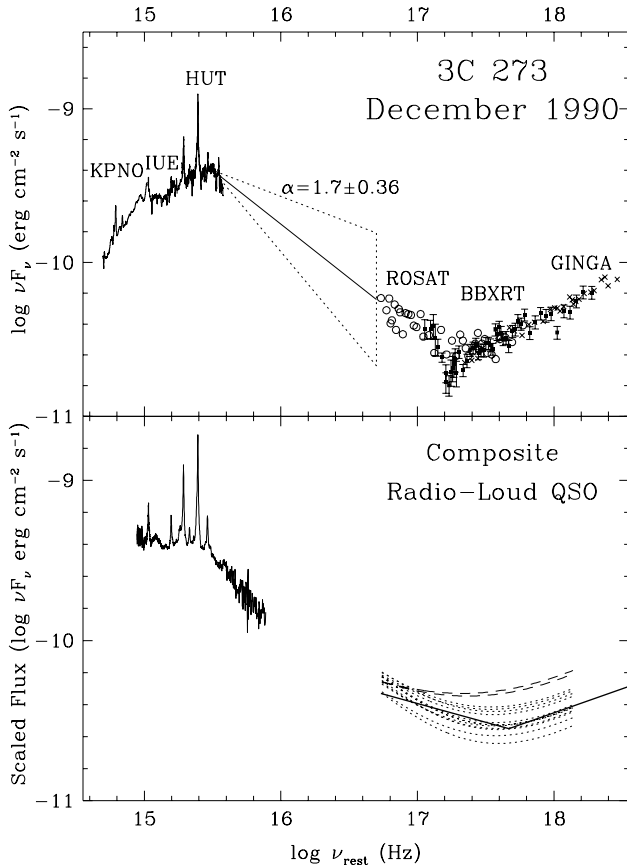


FIG. 6.— *Upper panel:* Quasi-simultaneous broad-band spectrum of 3C 273 from optical to X-rays obtained in December 1990, corrected to the rest frame. The ultraviolet and optical data have been corrected for reddening with $E(B-V) = 0.032$, and the ROSAT and BBXRT data have been corrected for interstellar absorption with $N_H = 1.84 \times 10^{20} \text{ cm}^{-2}$. To show the continuum shape more clearly, the UV and optical data have been smoothed with a 9-pixel boxcar filter. The best-fit power law for the short wavelength HUT data with $\alpha = 1.7$ is indicated, along with 1σ uncertainties for the slope. *Lower panel:* Composite radio-loud quasar spectrum in the UV-optical from Zheng et al. (1997) and in the X-ray from Laor et al. (1997). The UV-optical spectrum has been scaled to match the flux of 3C 273 at 1000 \AA , near the break found in the composite spectrum (1050 \AA rest) and in the 3C 273 spectrum (919 \AA rest). The X-ray spectrum has been scaled to the UV-optical composite using the mean α_{ox} for the Laor et al. sample. The dotted and dashed curves represent the spectral fits to 14 observations of 3C 273 over a 30-day period with ROSAT (LMP95). All but two of these observations (dashed) gave $\alpha_{\text{soft}} = 1.64 - 1.78$.

Finally we have also plotted the results of an extensive set of observations of 3C 273 with ROSAT in 1992 December to 1993 January by LMP95. These authors obtained spectra at 2-day intervals over a period of a month. They found that the only successful fits to their spectra were obtained with a sum of two power laws, where they constrained the hard component to have $\alpha_h = 0.5$ as determined by EXOSAT and *Ginga* 2–10 keV observations, and also constrained the interstellar absorption at low energies to be given by the Galactic value of $N_H = 1.84 \times 10^{20} \text{ cm}^{-2}$. Their soft component was then found to have $\alpha_s = 1.7$ for all but two of their observations, where they found $\alpha_s = 1.4$. We have plotted the fits given in Table 6 of LMP95 as dotted-line curves in Fig. 6, with the two discrepant observations as dashed-line curves. It is immediately apparent that these observations of 3C 273 match quite well the composite radio-loud X-ray spectrum of Laor et al. (1997) as we have scaled it to match the UV-optical composite, which itself was scaled to match our observation of 3C 273 at 1000 \AA . They are

also seen to extrapolate very well to match the extreme ultraviolet part of our composite UV-optical spectrum (Zheng et al. 1997).

The upper panel of Fig. 6 thus demonstrates the ultraviolet peak in the energy distribution of a single quasar, 3C 273, and a likely power-law connection extending from the Lyman limit to the soft X-ray region, with $\alpha_{\text{EUV}} = 1.7 \pm 0.36$, though a substantial extreme ultraviolet gap necessarily remains unfilled. The lower panel of Fig. 6, on the other hand, makes use of composite quasar spectra constructed in the UV-optical and the X-ray regions (suitably scaled) along with soft X-ray data for 3C 273 (LMP95), to reveal a very similar spectrum, with a significantly smaller extreme ultraviolet gap remaining unfilled.

The striking similarity between the 3C 273 spectrum and the spectral composite provides genuine physical support for the reality of the composite spectral shape derived by Zheng et al. (1997). (We note that 3C 273 made no contribution to the shape of the composite as only quasars with $z > 0.33$ were included in the sample used.) One can argue that composite spectra in and of themselves are unphysical. Zheng et al. (1997) note that there is a wide dispersion in spectral indices among individual quasars. Koratkar & Blaes (1999) show several examples of widely differing QSO spectral shapes. So, there is no guarantee that the composite assembled by Zheng et al. (1997) actually represents a real spectrum. The fact that the spectrum of a single object such as 3C 273 exhibits such remarkably similar characteristics bolsters the case for the broad applicability of the composite spectrum. Taken together, the composite spectrum and the 3C 273 spectrum provide compelling evidence for a power-law spectrum from the Lyman limit to the soft X-ray band in quasars, with a typical value of $\alpha = 1.7 - 2.2$.

5. ACCRETION DISK MODELS

To place our empirical results on the continuum spectral shape of 3C 273 in a physical context, we compare our spectra to accretion disk models. Such models are well suited to producing spectra that peak in the far-UV, and the spectral break near the Lyman limit in the quasar rest frame suggests a mechanism related to the large change in opacity at the intrinsic Lyman edge. The presence of a break rather than an edge, however, plus the seeming extrapolation of the high-frequency power law to soft X-ray energies are suggestive of the appearance of an accretion disk spectrum with an intrinsic Lyman edge feature that has been Comptonized by an external medium. Comptonization (and relativistic effects in the disk) smear out any intrinsic features in the disk spectrum as well as adding a power-law high-energy tail (Czerny & Zbyszewska 1991). As we will note below, however, the observed break is still sharper than what can be accommodated by our simple, semi-empirical models.

To fit the broad-band spectral shape, we compute disk spectra in the Schwarzschild metric that are a sum of blackbody spectra representing rings in the disk running from an inner radius of 6 gravitational radii ($r_G = GM_{\text{BH}}/c^2$) to $1000 r_G$. The blackbody spectra are modified by an empirical Lyman-limit feature as described by Lee, Kriss, & Davidsen (1992) and Lee (1995). For the Comptonization we assume that a hot spherical medium with an optical depth to Compton scattering of $\tau_e = 1$ surrounds the disk. We use the formulation of Czerny & Zbyszewska (1991) as described by Lee, Kriss, & Davidsen (1992) to calculate the effects of the Comptonization. The spectral index of the high energy tail in this calculation depends almost entirely on the Compton y parameter, $y \propto \tau_e^2 T_e$, where

T_c is the temperature of the Comptonizing medium (Lee 1995), so the free parameters in our accretion disk model are the mass accretion rate, \dot{m} , the mass of the central black hole, M_{BH} , the optical depth at the Lyman edge, τ_{Ly} , the inclination of the disk, i , and T_c (since we keep τ_e fixed at 1).

Our fits use the same wavelength intervals as the power-law and broken power-law fits in §3.2 and the same emission and absorption components. All fits have the extinction fixed at $E(B-V) = 0.032$. Since there is little data in our HUT spectrum shortward of the spectral break at ~ 920 Å in the rest frame, it is the slope and intensity of the soft X-ray spectrum that largely determines T_c . This has a best fit value of $T_c = 4.1 \times 10^8$ K in all our fits, regardless of the other parameters. The shape of the intrinsic disk spectrum is invariant for a fixed ratio of \dot{m}/M_{BH}^2 ; this ratio is determined largely by the wavelength of the peak in the spectral energy distribution. The normalization is determined by the mass accretion rate \dot{m} . For conversion of flux to luminosity, we assume a Hubble constant $H_0 = 75$ km s $^{-1}$ Mpc $^{-1}$ and a deceleration parameter $q_0 = 0$. The strength of the spectral break in our model is related both to the peak in the spectral energy distribution as well as the optical depth at the Lyman edge, τ_{Ly} . The break wavelength and its sharpness constrain the best fit inclination i . (Higher inclinations lead to breaks at shorter wavelengths that are more smeared out.)

Our best fit to the Astro-1 spectrum, for which simultaneous X-ray data and nearly simultaneous near-UV and optical data are also available, yields $\chi^2 = 1609$ for 1622 data points and 82 free parameters. The best-fit parameters are summarized in the first column of Table 8. (The emission and absorption line parameters have nearly identical values to those presented from our previous empirical fits.) The quoted errors are 90% confidence for a single interesting parameter, and they correspond to $\Delta\chi^2 = 4.6$. The Comptonized accretion disk fits significantly better than a single power law at the nominal value for Galactic extinction, but worse than the best fitting broken power law. The sharp break present in the spectrum is difficult to match with the smoother shape of our simple accretion disk model, even with a Lyman-limit feature.

TABLE 8 ACCRETION DISK MODELS FOR 3C 273		
Parameter	Astro-1	Astro-2
M_{BH} ($10^8 M_\odot$)	7.1 ± 0.3	12 ± 0.4
\dot{m} ($M_\odot \text{ yr}^{-1}$)	13 ± 0.13	12 ± 0.12
i (deg)	60^{+20}_{-10}	60^{+25}_{-40}
τ_{Ly}	0.5 ± 0.5	$0.0^{+0.2}_{-0.0}$
T_8 (10^8 K)	4.1 ± 0.2	4.1 ± 0.2
$E(B-V)$	0.032	0.032
χ^2/dof	1609/1540	1752/1497

The best fit to the Astro-2 spectrum is also summarized in Table 8. The most significant difference between the Astro-1 and the Astro-2 fits is that since the Astro-2 spectrum is redder overall, its fit favors a higher mass black hole. In all other respects, however, the Astro-1 and Astro-2 disk fits are similar. Reflecting the nearly identical flux levels of the two observations, the mass accretion rates are comparable. Both fits favor an inclination $i = 60^\circ$, and the Lyman-limit optical depth in each is low. For Astro-1, $\tau_{Ly} = 0.5$, and $\tau_{Ly} = 0.0$ also gives an acceptable fit; for Astro-2, $\tau_{Ly} = 0.0$. Thus in the context of our simple accretion disk model a Lyman edge feature is not formally required to achieve an acceptable fit to our data for either Astro-1 or Astro-2. However, the fact that a broken power-law actually

provides a better fit, and that the break is very close to the Lyman limit, hints that there probably is an effect associated with an opacity change at the Lyman limit. We suggest that future more sophisticated disk models should endeavor to match this feature.

Fig. 7 shows the best-fit accretion disk spectrum in comparison to the HUT Astro-1 data and longer-wavelength points. Here one can see that the rather smooth disk model does not fully accommodate the sharp spectral break at ~ 1000 Å. In the near-UV range the accretion disk continuum falls below the data largely due to Balmer continuum and Fe II line emission that is not included in our model. At longer wavelengths, the accretion disk falls below the data even more as we have not included any emission components (either a power law or dust emission) that are mainly responsible for the near-IR continuum. Fig. 8 again shows the best fit over the whole frequency range from the hard X-ray to 7000 Å in the visible. The Comptonized tail of the accretion disk spectrum provides an excellent match to the soft X-ray excess present in the ROSAT and the BBXRT data.

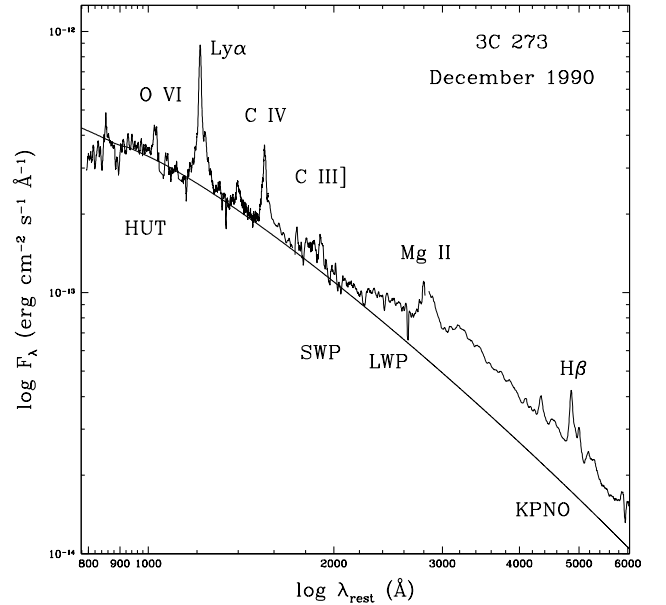


FIG. 7.— Quasi-simultaneous UV-optical spectrum of 3C 273 from 1990 December, including data from HUT, IUE, and the KPNO 2.1 m telescope (kindly provided by R. Green), corrected for reddening with $E(B-V) = 0.032$. The data have been smoothed with a 9-pixel boxcar filter. The smooth curve is the best-fitting accretion disk model as described in Section 5, with parameters given in Table 8.

Several aspects of our accretion disk fits illustrate the shortcomings of our simple model. Our best-fit inclinations of $i = 60^\circ$ are a bit high given the superluminal jet in 3C 273 that suggests the disk normal should be directed close to our line of sight. However, inclinations in superluminal sources can be as high as $30 - 45^\circ$, and this provides an acceptable fit for our Astro-2 observations. An inclination of 0° is excluded at high confidence in both data sets ($\Delta\chi^2 = 27$ for the Astro-1 data). Also, as mentioned earlier, the inclination is determined mostly by the wavelength of the spectral break. A Kerr disk would produce bluer breaks that are more smeared out at much lower inclination than in a Schwarzschild disk (e.g., see Laor & Netzer 1989).

Both the Astro-1 and Astro-2 fits have accretion rates that

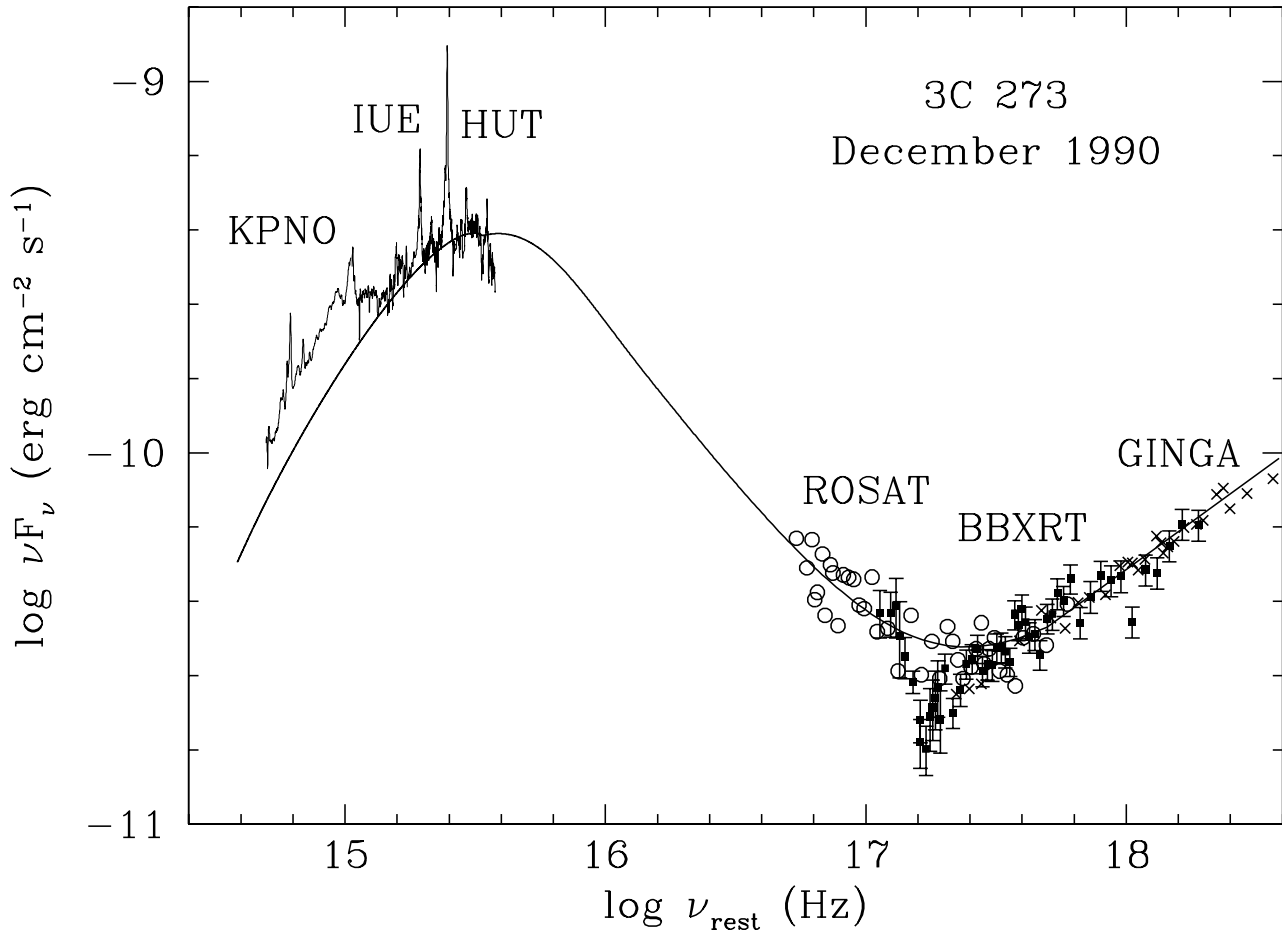


FIG. 8.— Quasi-simultaneous broad-band spectrum of 3C 273 as described in Fig. 5, with the best-fitting Comptonized accretion disk model added to a hard X-ray power-law with $\alpha = 0.5$. The sharp turn downward of the observed data below the model at the shortest ultraviolet wavelengths is simply absorption by the converging hydrogen Lyman series, and it is fully accounted for in our models (see Fig. 3).

exceed the thin-disk limit of $L/L_{Edd} \sim 0.3$ for a Schwarzschild metric. For the Astro-1 fit, $L/L_{Edd} = 0.46$; for Astro-2, $L/L_{Edd} = 0.25$. A Kerr metric would also alleviate this problem: the limit for a thin disk in this metric is higher, and, at the lower inclinations it would require, the accretion rate would also be lower.

Finally, while the Astro-1 and Astro-2 fits have similar mass accretion rates, their best-fit black hole masses differ by nearly a factor of two. This illustrates a fundamental difficulty of simple steady-state accretion disk models in dealing with variability: it occurs on time scales more rapid than the viscous time scale that governs the applicability of steady-state models. In a steady-state model for a given object, the only variable that can vary freely is the mass accretion rate. Therefore, one should observe correlated changes in flux and color, with brighter states exhibiting bluer disk spectra. However, the Astro-1 and Astro-2 data are nearly identical in flux, but they have significantly different colors. Without a good model for accommodating variability in disk models, one can see that factors of several uncertainty in the actual physical parameters are easily present in our results. It is reassuring to note, however, that our values for the black hole mass based on accretion disk models ($7.1 - 12 \times 10^8 M_\odot$) bracket the independent value of $7.4 \times 10^8 M_\odot$ obtained by Laor (1998) using reverberation-

mapping data.

We conclude that our accretion disk models of the Astro-1 and Astro-2 spectra provide an overall qualitative physical characterization of the 3C 273 spectrum. While the models have quantitative shortcomings, they provide an empirical guide for potentially more sophisticated models. The most important aspects of our simple description in terms of blackbody emission and Comptonization are that it (1) accounts for the peak of the ultraviolet spectrum, (2) produces a spectral break in the far-UV, and (3) has a hard power-law tail that extends to the soft-X-ray band and matches the observed soft-X-ray spectrum.

6. SUMMARY

We have presented absolutely-calibrated ultraviolet spectrophotometry over the 900–1800 Å range for the quasar 3C 273, obtained with the Hopkins Ultraviolet Telescope on the Astro-1 mission in December 1990 and on the Astro-2 mission in March 1995. In both observations the continuum displays a change of slope near the Lyman limit in the quasar rest frame. At longer UV wavelengths the continuum is well-represented by a power-law of $\alpha_1 = 0.5$. Shortward of the Lyman limit, however, the continuum slope has $\alpha_2 = 1.7 \pm 0.36$, where the uncertainty includes our uncertainty about $E(B-V)$ at the level of ± 0.01 .

The energy distribution per logarithmic frequency interval νf_ν therefore has a peak close to the quasar Lyman limit. The short wavelength extreme UV power-law extrapolates very well to match the soft x-ray spectrum of 3C 273 obtained nearly simultaneously in the case of Astro-1 with BBXRT and ROSAT. The soft x-ray data themselves give $\alpha_s = 1.7(\pm 0.1)$ (LMP95), so the combined UV and X-ray data suggest $\alpha_{UV-X} = 1.7$. While some models for the photoionizing extreme ultraviolet radiation from quasars have a peak — the so-called “big blue bump” — at a wavelength much shorter than the Lyman limit at 912 Å with a peak flux much higher than what is actually observed at both longer and shorter wavelengths (e.g., Mathews & Ferland 1987; Bechtold et al. 1987; Gondhalekar et al. 1992), we find that in 3C 273 the peak of the big blue bump occurs very close to the Lyman limit. The photoionizing flux from 3C 273 is given by $f_\nu = f_{LL}(\nu/\nu_{LL})^{-1.7}$ extending from the Lyman limit to 1 keV, although there is still a gap in the data covering one decade of frequency in the extreme ultraviolet.

Analysis of composite quasar spectra constructed in the ultraviolet (Zheng et al. 1997) and the X-ray (Laor et al. 1997) bands leads to the same result. The similarity between the spectrum of a single object such as 3C 273 and these composites lends physical credence to their applicability. It therefore appears to be true of quasars in general that the peak of the continuum energy distribution occurs near the Lyman limit, and that the ionizing continuum is well-represented by a power-law of energy index $\alpha_{UV-X} = 1.7 - 2.2$ extending to about 1 keV, where a separate hard X-ray component begins to dominate for higher energies. The “extreme ultraviolet gap” in the composite quasar spectrum is now only half a decade in frequency, however. This can be reduced somewhat further by extending the work of Zheng et al. (1997) to include more observations of high redshift quasars in the far ultraviolet band.

The general shape of the optical, ultraviolet, and soft x-ray spectrum of 3C 273 is consistent with that of an optically thick accretion disk around a massive black hole, which is itself surrounded by a hot medium that modifies the emergent spectrum through the inverse Compton effect, as suggested by Czerny &

Zbyszewska (1991), Lee et al. (1992) and Lee (1995). In our model the spectral break is due to the thermal peak of the accretion disk spectral energy distribution with a minor contribution from Lyman edge absorption. Both features are broadened and blurred by Comptonization in a surrounding hot medium, perhaps a corona or wind emanating from the disk. Comptonization of the thermal photons from the disk also produces the power-law tail extending to the soft X-ray region (e.g., Czerny & Elvis 1987; Maraschi & Molendi 1990; Ross, Fabian, & Mineshige 1992). Our simple model is unable to fully account for the sharpness of the spectral break, however, and we suggest that a more sophisticated treatment of the Lyman-edge region may eventually provide a better match to these data.

Assuming a Schwarzschild black hole with an inclination of 60 degrees, the UV spectrum is fit with a black hole mass $M_{bh} = 7 \times 10^8 M_\odot$ with an accretion rate $\dot{M} = 13 M_\odot/\text{yr}$. Superposed on the disk spectrum is an empirically determined Lyman edge with $\tau_{Ly} = 0.5$. The hot corona or wind is required to have a Compton parameter $y \approx 1$, which is obtained, for example, with $\tau_{es} = 1$ and $T_e = 4 \times 10^8$ K. A temperature of this order appears plausible for a corona where Compton cooling balances Compton heating by the hard x-ray flux in 3C 273. These results are quite similar to those we found previously by fitting similar models to a composite quasar spectrum (Zheng et al. 1997). There we found, assuming a typical inclination of 30 degrees, a black hole mass $M_{bh} = 1.4 \times 10^9 M_\odot$ and an accretion rate $\dot{M} = 2.8 M_\odot/\text{yr}$. While the best-fit parameters would change somewhat in the more realistic case of a rotating (Kerr) black hole (which we have not calculated), we believe these results provide strong evidence in favor of the hypothesis that quasars are powered by accretion onto massive black holes.

We thank R. Green for providing the optical data, J. Kruk and C. Bowers for help with the Astro-1 data, and K. Weaver for assistance with the X-ray data reduction. The Hopkins Ultraviolet Telescope project has been supported by NASA contract NAS-5-27000 to the Johns Hopkins University.

REFERENCES

- Appenzeller, I. et al. 1998, *ApJ*, 500, L9
 Arnaud, K. A. 1996, in *ASP Conf. Series 101, Astronomical Data Analysis Software and Systems V*, ed. G. Jacoby & J. Barnes, (San Francisco: ASP) 17
 Arnaud, K. A., et al. 1985, *MNRAS*, 217, 105
 Bahcall, J. N., Jannuzi, B. T., Schneider, D. P., Hartig, G. F., Bohlin, R., & Junkkarinen, V. 1991, *ApJ*, 377, L5
 Baldwin, J. A. 1975, *ApJ*, 201, 26
 Bechtold, J., Czerny, B., Elvis, M., Fabbiano, G., and Green, R. F. 1987, *ApJ*, 314, 699
 Bowyer, C. S., Lampton, M., Mack, J., & de Mendonca, F. 1970, *ApJ*, 161, L1
 Cardelli, J., Clayton, G., & Mathis, J. 1989, *ApJ*, 345, 245
 Courvoisier, T.J.-L., et al. 1987, *A&A*, 176, 197
 Czerny, B. & Elvis, M. 1987, *ApJ*, 321, 305
 Czerny, B. & Zbyszewska, M. 1991, *MNRAS*, 249, 634
 Davidsen, A. F., Hartig, G. F. & Fastie, W. G. 1977, *Nature*, 269, 203
 Davidsen, A. F., et al. 1992, *ApJ*, 392, 264
 Done, C. 1993, *Adv. Space Res.*, 13, 12211
 Gondhalekar, P. M., Pounds, K. A., Sembay, S., Sokoloski, J., Urry, C. M., Mathews, L., & Quenby, J. 1992, in *Physics of Active Galactic Nuclei*, ed. W. J. Duschl & S. J. Wagner, (Berlin: Springer), 52
 Haardt, F., & Madau, P. 1996, *ApJ*, 461, 20
 Hurwitz, M., et al. 1998, *ApJ*, 500, 61
 Koratkar, A., & Blaes, O. 1999, *PASP*, 111, 1
 Kriss, G. A. 1994, in *Astronomical Data Analysis Software and Systems III*, A.S.P. Conf. Series, V. 61, ed. D. R. Crabtree, R. J. Hanisch & J. Barnes (San Francisco: ASP), 437
 Krolik, J. H., & Kallman, T. R. 1988, *ApJ*, 324, 714.
 Kruk, J. W., Durrance, S. D., Kriss, G. A., Davidsen, A. F., Blair, W. P., Espey, B. R., & Finley, D. S. 1995, *ApJ*, 454, L1
 Kruk, J. W., et al. 1997, *ApJ*, 482, 546
 ———, 1999, *ApJS*, 122, 299
 Laor, A. 1998, *ApJ*, 505, L83
 Laor, A., Bahcall, J. N., Jannuzi, B. T., Schneider, D. P., & Green, R. F. 1995, *ApJS*, 99, 1
 Laor, A., Fiore, F., Elvis, M., Wilkes, B. J., & McDowell, J. C. 1997, *ApJ*, 447, 93
 Laor, A., & Netzer, H. 1989, *MNRAS*, 242, 560
 Leach, C. M., McHardy, I. M. & Papadakis, I. E. 1995, *MNRAS*, 272, 221 (LMP95)
 Lee, G. 1995, Ph.D. thesis, the Johns Hopkins University
 Lee, G., Kriss, G. A., & Davidsen, A. F. 1992, in *Testing the AGN Paradigm*, ed. S. S. Holt, S. G. Neff, & C. M. Urry (New York: AIP), 159
 Lichti, G. G., et al. 1995, *A&A*, 298, 711
 Lynden-Bell, D. 1969, *Nature*, 223, 690
 Malkan, M. A. 1983, *ApJ*, 268, 582
 Malkan, M. A. & Sargent, W. L. 1982, *ApJ*, 254, 22
 Maraschi, L., & Molendi, S. 1990, *ApJ*, 353, 452
 Masnou, J. L., Wilkes, B. J., Elvis, M., McDowell, J. C., & Arnaud, K. A. 1992, *A&A*, 253, 35
 Mathews, W. G., & Ferland, G. J. 1987, *ApJ*, 323, 456
 Morris, S. L., Weymann, R. J., Savage, B. D., & Gilliland, R. L. 1991, *ApJ*, 377, L21
 Morrison, R., & McCammon, D. 1983, *ApJ*, 270, 119
 O’Brien, P. T., Gondhalekar, P. M., & Wilson, R. 1988, *MNRAS*, 233, 801
 Reichert, G. A., Polidan, R. S., Wu, C.-C. & Carone, T. E. 1988, *ApJ*, 325, 671
 Ross, R. R., Fabian, A. C., & Mineshige, S. 1992, *MNRAS*, 258, 189
 Serlemitsos, P. J., et al. 1992, in *Frontiers of X-ray Astronomy*, ed. Y. Tanaka & K. Koyama (Tokyo: Universal Academy Press), 221
 Shields, G. 1978, *Nature*, 272, 706

- Staubert, R. et al. 1992, in Testing the AGN Paradigm, ed. S. S. Holt, S. G. Neff, & C. M. Urry, (New York: AIP), 366
- Turner, M. J. L., Courvoisier, T.J.-L., Staubert, R., Molteni, D., & Trumper, J. 1985, Space Sc. Rev., 40, 623
- Turner, M. J. L., et al. 1990, MNRAS, 244, 310
- Turner, T. J., & Pounds, K. A. 1988, MNRAS, 232, 463
- Turner, T. J., Weaver, K. A., Mushotzky, R. F., Holt, S. S., & Madejski, G. M. 1991, ApJ, 381, 85
- Worrall, D. M., Mushotzky, R. F., Boldt, E. A., Holt, S. S., & Serlemitsos, P. J. 1979, ApJ, 232, 683
- Wilkes, B. J., & Elvis, M. 1987, ApJ, 323, 243
- Zheng, W. Kriss, G. A., Telfer, R. C., Grimes, J. P. & Davidsen, A. F. 1997, ApJ, 475, 469
- Zheng, W., & Malkan, M. A. 1993, ApJ, 415, 517